Journal of
Applied Crystallography
ISSN 0021-8898

Extraction of domain structure information from small-angle scattering patterns of bulk materials

Norbert Stribeck

Journal of
Applied Crystallography
ISSN 0021-8898

Received 31 July 2000
Accepted 9 April 2001

Dedicated to Professor Dr W. Ruland on the occasion of his 75th birthday.

Extraction of domain structure information from small-angle scattering patterns of bulk materials

Norbert Stribeck

Universität Hamburg, Institut f. Techn. u. Makromol. Chemie, Bundesstr. 45, 20146 Hamburg, Germany. Correspondence e-mail: norbert.stribeck@desy.de

A method is presented that permits the extraction and visualization of topological domain structure information contained in small-angle scattering (SAS) patterns without complex pretreatment. Multi-dimensional noisy raw data can be processed. Such data are, for instance, accumulated in the field of materials research from short-exposure-time *in situ* small-angle X-ray scattering (SAXS) experiments with synchrotron radiation. The result is a multi-dimensional intersect or chord distribution, which is defined as the Laplacian of the correlation function. Moreover, it is equivalent to the autocorrelation of the gradient of the electron density. The procedure is, in particular, adapted to the analysis of the nanoscale structure of samples with fibre symmetry, such as polymer fibres or strained elastomers. Multi-dimensional relations among morphological components become apparent in real space and help to elucidate the nature of the processes governing formation and change of structure on the nanometre scale. Utilizing digital signal processing tools, the algorithm is based on spatial frequency filtering of the raw data. The background to be subtracted from the small-angle scattering pattern is formed from its own low spatial frequencies. Noise may be removed by suppressing high spatial frequencies. In the frequency band between these low and high spatial frequencies, the domain structure information of the studied nanocomposite appears.

1. Introduction

The extraction of structural data from small-angle scattering patterns has been a problem of constant interest to researchers for many years, particularly in the field of bulk polymer materials. Raw experimental data are inexact and, moreover, describe a physical structure which can only be modelled imperfectly. It is common practice to eliminate apparent effects after measuring the detector characteristics, the blind scattering and the sample absorption. What remains is, in general, the scattering pattern of a non-ideal multi-phase system. Single-phase or fractal systems will not be considered in this paper. Moreover, the study does not claim to focus on isotropic dilute or liquid materials, for which background of different nature is corrected by established experimental methods.

Deviations from an ideal multi-phase structure have been discussed for many years (Ruland, 1971; Wolff *et al.*, 1994; Ruland, 1987; Siemann & Ruland, 1982; Ciccariello, 1985; Ciccariello & Benedetti, 1986; Stribeck *et al.*, 1997). Fluctuation of the electron density inside the phases, for instance, causes a slowly varying background in the scattering data (Ruland, 1971). The decay of the scattering intensity resulting from Porod's law (Porod, 1951) is increased by a smooth transition zone at the phase boundary (Ruland, 1971), and added roughness of the boundary itself raises the specific surface (Ruland, 1987). These slowly varying effects are superimposed in the scattering pattern. In isotropic data they can only be separated after resorting to extensive assumptions, and whenever anisotropic scattering data are to be analysed, these ambiguities become even more elusive. When two-dimensional scattering patterns from samples with fibre symmetry have been studied quantitatively, the work has been restricted to the analysis of curves extracted from the scattering patterns (Bonart, 1966; Stribeck, 1999, 2000; Stribeck *et al.*, 1999; Cohen & Thomas, 1987; Hall *et al.*, 1987; Hall & Hussain, 1990; Kumar *et al.*, 1994), which only reflect partial aspects of the domain structure.

The presented method points at a solution of the aforementioned problems, in so far as a multi-phase system is to be studied. Assessment concerning short-range fluctuations of electron density as well as such concerning the width of the interfacial layer between the domains cannot be made.

Closely related to the work presented here is a recent publication (Elliot & Hanna, 1999) presenting a method for the generation of a domain-structure picture from a small-angle scattering pattern. The authors present a maximum-entropy algorithm on Shannon's entropy with respect to the electron density map in real space. The result of the algorithm is an image of one of the most probable electron density distributions, which in a two-dimensional universe would generate the observed two-dimensional scattering pattern.

2. Multi-dimensional chord distributions from SAS patterns

2.1. Overview

Whenever scattering methods are utilized, data are recorded in reciprocal space. From these data, structural information in physical space can be gained. Each effect, which in the scattering pattern is manifested as a slowly varying function, can be assigned to low spatial frequencies in physical space. Counting statistics, on the other hand, is most clearly apparent at high spatial frequencies. Thus, the accessible structural information of a scattering pattern is contained in a spatial frequency band between background frequencies and high-frequency noise. If an ambiguous image in physical space is not accepted, a (multi-dimensional) correlation function (Vonk & Kortleve, 1967; Vonk, 1979), an interface distribution function (IDF) (Ruland, 1977, 1978; Stribeck, 1993) or a chord distribution (Glatter & Kratky, 1982; Méring & Tchoubar, 1968) may be computed. According to the previous considerations, such an image is computed in three automatable steps: (i) proper transformation of the scattering pattern, (ii) band-pass filtering and (iii) Fourier transformation. Thus, now the choice of filter characteristics must be discussed and takes the place of a discussion of deviations from the ideal multi-phase model. Considering the new paradigm, the effect of smoothing the scattering pattern by a band-pass filter on the morphology acquires a novel meaning. The upper edge of the filter defines a distance in real space, beyond which no information on correlations among domains can be retrieved. Hence, the main effect of noise reduction by prolonged exposure is increased information on long-range order.

2.2. Definitions

Let $I(\mathbf{s})$ be the observed SAS intensity. The magnitude of the scattering vector can be defined by $|\mathbf{s}| = (2/\lambda)\sin\theta$, with λ the wavelength of radiation and 2θ the scattering angle. Common notations will be used for both the case of isotropic scattering patterns, by writing $I(\mathbf{s}) = I(s)$ with $s = |\mathbf{s}|$, and for the case of a scattering pattern with fibre symmetry, $I(\mathbf{s}) = I(s_{12}, s_3)$ with $s_{12} = (s_1^2 + s_2^2)^{1/2}$ and the direction of s_3 defining the symmetry axis of the pattern.

For the two cases mentioned, it can frequently be guaranteed that the recorded information on the structure is complete. In the isotropic case, the complete SAS information is contained in a curve. If in the case of fibre symmetry the tangent plane approximation is assumed to be valid, the complete SAS information is contained in a two-dimensional pattern, which can be recorded using a two-dimensional detector. Additionally, the researcher has to contribute to completeness, in so far as relevant information must not be hidden by the primary beam stop, and in the peripheries of the pattern the Porod region must have been recorded.

2.3. Intensity projection onto a plane

If the scattering pattern is already complete in a subspace of the three-dimensional reciprocal space, the suitable projection (Bonart, 1966; Stribeck, 1992, 1999, 2000) has to be carried out before the following one-dimensional or two-dimensional Fourier transformation. In classical methods, special Fourier kernels are employed, which comprise the projection implicitly. For the data evaluation of scattering 'images' with fibre symmetry, it is convenient to utilize commercial standard software for image processing, such as *pv-wave* (1997), *IDL* (1999) or *Matlab* (2000), to carry out the necessary projection

$$I_P(s_1, s_3) := \{I(s_{12}, s_3)\}(s_1, s_3) = \int I(s_{12}, s_3)\,\mathrm{d}s_2, \qquad (1)$$

the two-dimensional Fourier transformation $\mathcal{F}^2(I_P)(r_{12}, r_3) := P(r_{12}, r_3)$ of which is known as the two-dimensional (electron-) density correlation function (Vonk, 1979) in cylindrical coordinates. Let us consider a correlation function computed from ideal model data and turned into a two-dimensional digital image. Then, anticipating the next subsection, the generalized chord distribution can be computed by convolution with the digital Laplacian operator (Haberäcker, 1989; Rosenfeld & Kak, 1982)

$$L_d = \begin{pmatrix} 0 & -1 & 0 \\ -1 & 4 & -1 \\ 0 & -1 & 0 \end{pmatrix}.$$

2.4. A generalized chord distribution

In the case of isotropic data, the features of the nanostructure can be visualized much more clearly in a chord distribution function (CDF) (Méring & Tchoubar, 1968) or in an interface distribution function (IDF) (Ruland, 1977) than in a correlation function. Now the question arises: how can the one-dimensional concepts of the CDF and the IDF be generalized for the case of multi-dimensional scattering data from multi-phase systems? Three approaches are presented here. The mathematical background of the only one which has proven its feasibility for the evaluation of experimental data is presented in Appendix *A*.

Projecting anisotropic scattering data onto (inclined) lines passing through the centre of the pattern appears to be the straightforward approach. After multiplication by s^2 and one-dimensional Fourier transformation, each curve gives the multi-dimensional CDF $g(r, \psi, \varphi)$ in a single direction, from which the total CDF can be constructed. Applied to ideal model data, this method works perfectly, but as soon as noise and background are added to model patterns, background separation becomes a problem. Then the missing 'connectivity' among the individual rays results in artifacts as a function of ray orientation, which are difficult to control.

As a second possibility, Burger & Ruland (2000) propose to define the generalized CDF by the second derivative of the correlation function with respect to r, the modulus of the vector in physical space. Pursuing this concept for the case of fibre symmetry obviously results in a solution made from three integral transforms. Based on this solution, no numerical

procedure has been found that is able to reproduce even the known result for the scattering of a sphere.

As deduced in Appendix *A*, the autocorrelation of the gradient of the density distribution can be defined as a chord distribution $z(\mathbf{r}) = [\nabla\rho(\mathbf{r})]^{*2}$ for any multi-dimensional case. It is equivalent to the Laplacian $\Delta P(\mathbf{r})$ of the correlation function and can be computed from the multi-dimensional Fourier transformation of the scattering intensity $I(\mathbf{s})$ after multiplication by $4\pi^2 s^2$. For samples with fibre symmetry, we start from the projected intensity I_P and obtain

$$I_L(s_1, s_3) = 4\pi^2 s^2 I_P(s_1, s_3) \tag{2}$$

with $s^2 = (s_1^2 + s_3^2)^{1/2}$ in this context.

In the next evaluation step, the non-ideal character of the studied multi-phase structure has to be considered. In the classical methods (Ruland, 1971, 1977; Stribeck & Ruland, 1978) this is accomplished by subtraction of several slowly varying backgrounds (density fluctuations, width of the phase transition, domain roughness). These backgrounds are well justified for physical reasons, but difficult to separate. The result of this operation is an interference function $G(\mathbf{s})$, which shall be subject to a Fourier transformation. Since our interest is not in the study of non-ideal character, but information on shape and arrangement of the nanometre-size domains, the composite slowly varying background in the SAS image is considered a parasitic effect which has to be eliminated. Obviously, a suitable background can be extracted from the SAS pattern itself by computing the low-pass-filtered pattern, $f_{\ell,r_c}[I_L(\mathbf{s})]$. Its subtraction reduces the central singularity in the Fourier transformation of $I_L(\mathbf{s})$. Hence an adapted interference function $G(\mathbf{s})$,

$$G(\mathbf{s}) = I_L(\mathbf{s}) - f_{\ell,r_c}[I_L(\mathbf{s})], \tag{3}$$

is defined based on a low-pass-filter operator $f_{\ell,r_c}(\,)$ with a cut-off frequency r_c. On the one hand, a background correction based on a low-pass filter is no more arbitrary than the background fitting methods commonly employed in the evaluation of small-angle scattering curves. On the other hand, the extension of low-pass filtering to multi-dimensional data is straightforward. Long experience in the evaluation of one-dimensional scattering data has shown that any background chosen with common sense yields very similar results for the values of the topology-related parameters.

Analogously, in the multi-dimensional case, a filter parameter variation shows that the final CDF is altered only marginally, as long as a filter with smooth frequency response is chosen and the cut-off frequency is kept low. For the commonly used Butterworth filter, this means that a low order has to be chosen in order not to imprint artifacts resulting from discontinuities of the filter response function. A first-order Butterworth filter,

$$f_{\ell,r_c}[I_L(\mathbf{s})] = \mathcal{F}^{-1}\{\mathcal{F}[I_L(\mathbf{s})](\mathbf{r})/(1 + r/r_c)^2\} \tag{4}$$

[$r = |\mathbf{r}|$; $\mathcal{F}(\,)$ designates the multi-dimensional Fourier transformation], has proved feasible in many fields of research. Application shows that the cut-off frequency r_c can be varied within a fairly wide range without change of the apparent topological parameters. Nevertheless, after background subtraction there remain intensity discontinuities at the circumference of the sensitive area of the detector. The general procedure to minimize the corresponding artificial undulations in real space is multiplication by an appropriate windowing function. Frequently the 'Hamming window' is used. As a result of its discontinuity, it produces visible artifacts in the evaluated images. A better choice is the 'Hann window' (Press *et al.*, 1992), which is sometimes called the 'Hanning operator' (*pv-wave*, 1997).

2.5. Noise filter

Whenever the original data have been measured with high accuracy (more than 10000 counts in the maximum) and have already been projected, filtering of the high-frequency noise is not necessary. But *in situ* measurements of crystallization or of straining processes frequently require short exposure intervals. Limited capacity of the currently available detectors then causes even the projected data to exhibit pronounced noise. In this case, it is recommended to employ a noise filter,

$$G_\ell(\mathbf{s}) = f_{\ell,r_c}[G(\mathbf{s})]. \tag{5}$$

For typical polymer materials, a noisy but complete interference function with an edge length of 512 pixels appears to be sufficiently smooth after application of a Butterworth low-pass filter with a cut-off frequency of $r_c = 30$ (in units of pixels). One has to bear in mind that after this filtering operation, in the final chord distribution, only the central area of approximately $\pm 2r_c$ is non-zero and contributes to the morphological information on the sample. Information concerning longer ranging order or bigger domains was eliminated by the statistical noise of the measured data. This means that, whenever a test measurement with long exposure shows that long-range order in the material is low, noise filtering will not cause loss of information. Middle-frequency noise cannot be eliminated. We have to assume that this kind of noise will become the reason for deviations between a statistical model and the real-space representation (*e.g.* chord distribution, correlation function) or that its amplitude remains small as compared with the signal amplitude. The latter assumption is plausible, because visual perception recognizes two pictures to be similar if their middle spatial frequencies match. An apparatus recording patterns in which the middle frequencies vary at random would not fulfil the criterion of reproducibility.

2.6. Discrete Fourier transformation

Finally, the interference function $G(\mathbf{s})$ or $G_\ell(\mathbf{s})$ is subject to a discrete Fourier transformation, which is available for almost any data evaluation package and named DFT or FFT. In order to increase spatial resolution, the pattern has to cover a wide area in $\mathbf{s}$. Because of the definition of $G(\mathbf{s})$, it is allowed and common practice in the field of digital image processing to expand with zero intensity data ('zero padding'). The DFT algorithm requests the centre of the pattern to be located in the centre of a corner pixel. Thus the pattern is moved, the

Fourier transformation carried out and the centre returned to its original position. The result

$$z(\mathbf{r}) = -\mathcal{F}[G(\mathbf{s})] \qquad (6)$$

is the chord distribution $z(\mathbf{r})$. Starting from (1), the projection $I_P(s_1, s_3)$ of a scattering pattern with fibre symmetry, a two-dimensional Fourier transformation yields the section of $z(r_1, r_3)$ in the (r_1, r_3) plane. Because of fibre symmetry, the equivalence $r_1 = r_{12}$ is valid. Thus the complete morphological information concerning size and arrangement of domains is right at hand in the physical-space function $z(r_{12}, r_3)$ after few evaluation steps.

The method has been tested using the model scattering functions of spheres, lamellae, rods and layer stacks, both with uniform dimension and with a statistical variation of the particle dimensions. It is stable even for noisy data. The deviation of the resulting CDF $z(\mathbf{r})$ and the ideal CDF $g(\mathbf{r})$ computed from perfect model data after projections onto inclined lines is small.

3. Example

3.1. Data evaluation steps

Fig. 1 shows the SAXS pattern of a poly(styrene-*b*-isoprene-*b*-caprolactone) tri-block copolymer. It is part of a stretching series recorded at HASYLAB, Hamburg, beamline A2. After an exposure time of 2 min, the signal-to-noise ratio is high. On the USAXS beamline BW4, the same data quality is obtained after an exposure time of 60 min. Shortening the exposure time by a factor of 20 and applying the aforementioned low-pass filter yields the same result concerning the domain structure. Detector characteristics and blind scattering have been considered. The image $I(s_{12}, s_3)$ is already centred, aligned and averaged over four quadrants. It is complete, because it covers a region wide enough both in s_{12} and in s_3 and no features are missing in its centre.

Fig. 2 shows the result of the projection (1) of the fibre scattering. This operation reduces the statistical noise in the data set considerably and concentrates intensity in the centre of the pattern. Anticipating Fourier transformation, this narrowed intensity distribution will result in a more extended

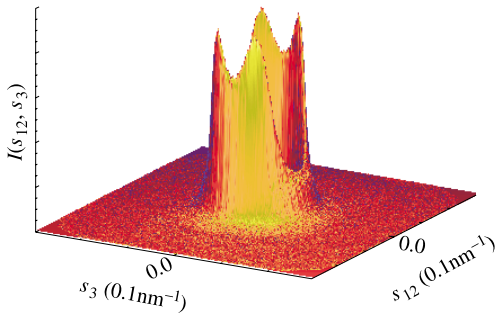

Figure 1
Two-dimensional SAXS pattern with fibre symmetry of an SICl tri-block copolymer at an elongation $\varepsilon = 0.5$, recorded at HASYLAB, Hamburg, beamline A2, on an image plate (2 min exposure) (range: $-0.15 < s_{12} < 0.15$ nm^{-1}, $-0.15 < s_3 < 0.15$ nm^{-1}).

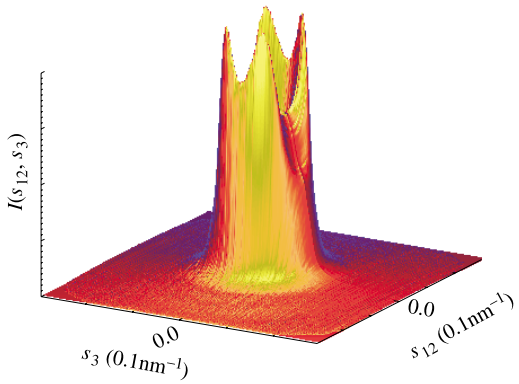

Figure 2
The projection $\int I(s_{12}, s_3)\,\mathrm{d}s_1$ of the fibre scattering intensity onto the (s_1, s_3) plane concentrates the intensity in the centre and smoothes the pattern.

pattern in physical space. After multiplication by s^2, the pattern shown in Fig. 3 is obtained. Fig. 4 shows the background extracted from the scattering pattern by application of a first-order Butterworth filter with a critical frequency of $r_c = 0.7$ in units as described in §2.5. The resulting pattern is shown in Fig. 5. Finally the Fourier transformation is applied, generating the complete chord distribution function of the domain structure. Fig. 6 presents a view of the upper face of this chord distribution, in which the inner peaks are associated with the domain size distributions whereas the outer peaks describe their mutual correlations within the fibre. Turning the chord distribution upside down would result in a view of the lattice face, in which the pronounced peaks are associated with the distributions of increasing orders of lattice constants.

3.2. Discussion of the result

The view in Fig. 6 mainly exhibits the pronounced broad domain thickness distributions, which indicate tilted layers with a certain orientation distribution. If, on the other hand, the chord distribution is viewed along the meridional direction (Fig. 7), a sequence of low-height peaks in the centre of the image reveals that there is a fraction of a second kind of domains, forming a structure perfectly oriented in the direction of strain and possessing low lateral extension. These

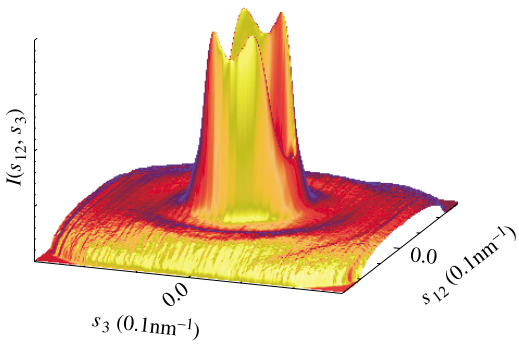

Figure 3
The projected intensity after multiplication by the second power of the distance from the centre of the pattern.

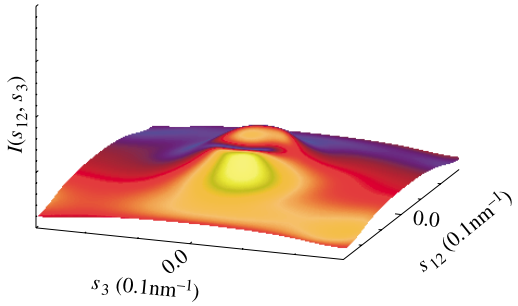

Figure 4
The background generated by extraction of the low spatial frequencies in the scattering pattern using a first-order Butterworth filter.

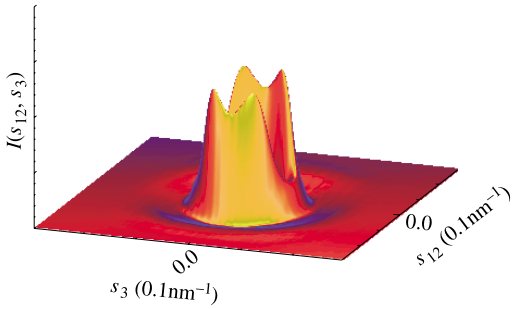

Figure 5
The interference function $G(s_1, s_3)$ is generated by subtraction of the filtered background function (*cf.* Fig. 4) from the pattern in Fig. 3 and application of the Hann window operator.

domains may be identified as hard domain cylinders aligned in a row along the fibre axis.

After interpreting the maxima of the chord distribution, one should also discuss the minima of the functions surface, which exhibit the different orders of the 'lattice constant'. They are best observed after turning the surface upside down. Viewed along the meridian, this 'lattice face' (Fig. 8), exhibits the peculiar orientation distributions of the 'long periods'. The rapid decay of the peaks as a function of their distance from the centre of the chord distribution reflects poor long-range

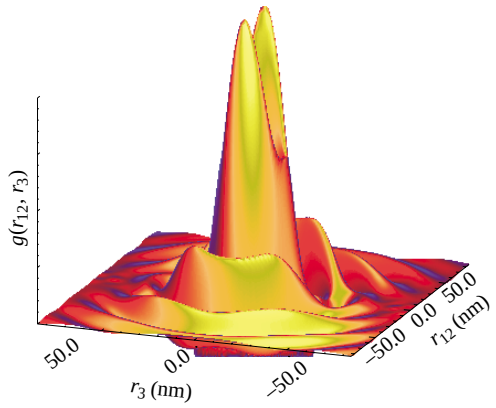

Figure 6
Three-dimensional Chord distribution $z(r_{12}, r_3)$ generated by Fourier transformation from the interference function $G(\mathbf{s})$. View of the 'domain' face seen almost perpendicular to the equator of the fibre.

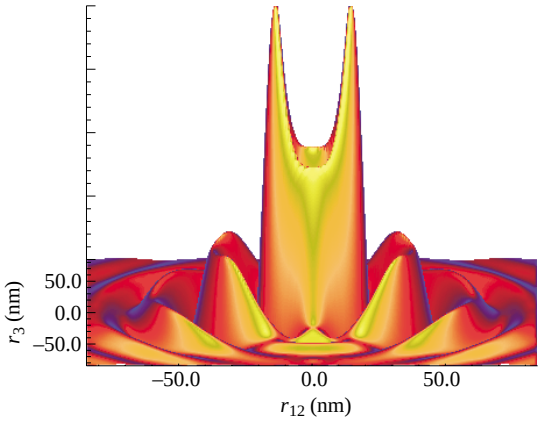

Figure 7
Chord distribution $z(r_{12}, r_3)$. Perspective of the 'domain' face viewed along the meridian of the fibre.

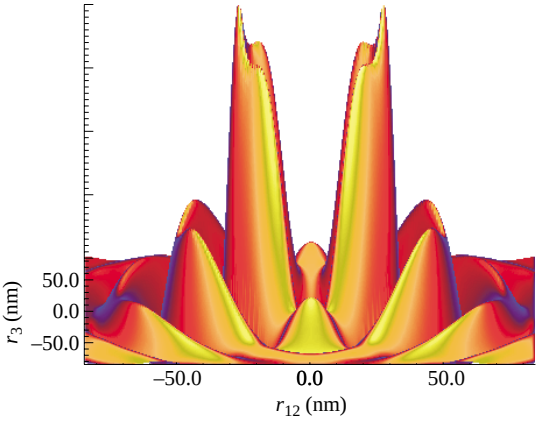

Figure 8
The chord distribution turned upside down ('lattice face') $-z(\mathbf{r})$, viewed along the meridian.

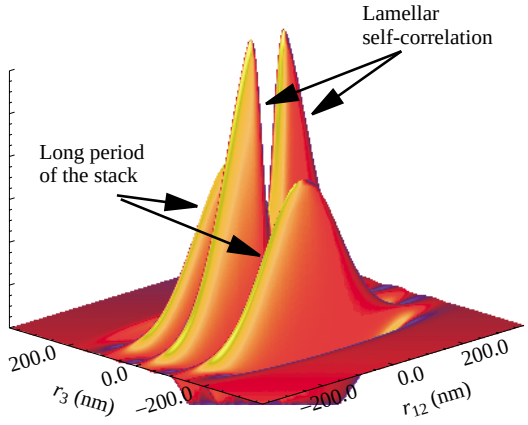

Figure 9
Model CDF $-z(\mathbf{r})$ from an ensemble of perfectly oriented stacks from two lamellae computed after one background-subtraction step. The central indentation in the 'lamellar self-correlation' is a result of background subtraction.

order of the nanostructure. At the equator, one observes a maximum in the first order, whereas the second and third order exhibit a relative minimum at the equator. Thus the range of the 'lattice' structure in the equatorial direction is much shorter than that of the structural component, which is formed by lamellae tilted with respect to the equator. All in all, the multi-dimensional chord distribution reveals the complex nanostructure of the polymer sample.

3.3. Discussion of the method

The example presented originates from a scattering pattern with pronounced peaks. Here the single subtraction of a two-dimensional low-pass background results in an unambiguous CDF, the features of which can hardly be modified by variation of the filter parameters. The result shall be named a 'CDF of the first kind'.

Sometimes, however, reflections in scattering patterns are only observable as shoulders on a monotonously decaying background. In this case, background subtraction has to be carried out iteratively, until the total integral of $G(\mathbf{s})$ vanishes. This procedure may be allowed if the presence of strongly distorted multi-phase nanostructures can be assumed. In this case, the iterative background subtraction removes 'roughness' from the domain surfaces, until a clear multi-phase structure remains and a 'CDF of the second kind' is obtained. Even if such a CDF appears to show clear features, they should be interpreted with caution. Confidence can be gained by comparison of many CDFs from a series in a continuous experiment. But even if a reasonable variation of the structure is observed, it remains questionable if the substantial aspects of the multi-phase structure have passed the cascade of spatial frequency filters.

Even more important is the implication of any background subtraction itself. It is based on the understanding that $z(0) = 0$, which means that there are no chords of zero length. Commonly, the self-correlation peak of the structure as a whole is considered to be a delta function at the origin. But for structures containing highly oriented domains, the self-correlation peak, in general, is not restricted to the vicinity of zero. Processing model scattering functions, one can easily demonstrate that the self-correlation of a lamella is a wide 'triangle' extending along the equator of the CDF, whereas the self-correlation of a rod is a wide triangle extending along the meridian. Background correction of scattering patterns has a strong effect on the central part of the CDF. Iterative background correction, in particular, will force the central part of self-correlation triangles to bend towards zero. The result in the CDF looks like a pair of strong correlation peaks on the lattice face of the CDF. Fig. 9 shows the lattice face of the model CDF from an ensemble of layer stacks made from two lamellae. The 'lamellar self-correlation' would look like a triangle, if no background subtraction were performed. As a result of the background subtraction, a central indentation is observed. Recursive background subtraction increases the artificial effect and may even cause visible attenuation of structural features in the CDF pattern.

4. Conclusions

The presented procedure only works with little user intervention if it is supplied with complete data. In this case it extracts the morphological information of SAS patterns within a minute and visualizes it in a clear physical-space representation, which is well suited for visual interpretation and, in the future, perhaps, even for quantitative analysis.

The qualitative analysis of the multi-dimensional chord distribution supplies the researcher with information on domain size, domain shape, domain orientation, range of order and, last but not least, on the number of components in the structure and their mutual arrangement in space. This information is valuable input for the design of an adapted structural model.

By fitting such a model to the scattering data, it should become possible to separate the components of the structure and quantitatively to describe their statistics, as has been performed in previous work for one-dimensional stacking statistics (Stribeck, 1993) and for one-dimensional projections from fibre patterns (Stribeck, 2000). If an *in situ* experiment is monitored by recording scattering patterns, the experimental parameters, like elongation, temperature or time, in conjunction with the observed structural changes, will help with the task of understanding the complexity of the morphologies which show up in multi-dimensional chord distribution functions. Moreover, the multi-dimensional relations among the components of a multi-component morphology may help to enlighten the nature of the processes governing structure formation and change in polymer materials on the nanometre scale.

APPENDIX *A*
The Laplacian of the correlation function

A1. The correlation function and its generating potential

Let $p(\mathbf{r}) = p(-\mathbf{r})$ be a correlation function generated from a potential $u(\mathbf{r})$ according to

$$p(\mathbf{r}) = u(\mathbf{r}) * u(-\mathbf{r}) := u^{*2}(\mathbf{r}) \tag{7}$$

(autocorrelation) with

$$f(\mathbf{r}) * h(\mathbf{r}) = \int_v f(\mathbf{y})\, h(\mathbf{y}-\mathbf{r})\, \mathrm{d}v_y$$

being the definition of the correlation. Here v designates volume integration. Let the Fourier transformation exist:

$$I(\mathbf{s}) = \mathcal{F}^3[p(\mathbf{r})] = \int_v p(\mathbf{r})\, \exp(2\pi i \mathbf{rs})\, \mathrm{d}v_r. \tag{8}$$

A2. Gradient of the potential and its autocorrelation

It can easily be shown that $(\nabla u)^{*2}(\mathbf{r})$, the autocorrelation of the gradient of the generating potential in Cartesian coordinates, is given by

$$(\nabla u)^{*2}(\mathbf{r}) = \sum_{i=1}^{3} \left(\frac{\partial u}{\partial r_i}\right)^{*2}(\mathbf{r}). \tag{9}$$

A3. The Fourier transformed terms

Let

$$U_i(\mathbf{s}) = \mathcal{F}^3\left[\frac{\partial u}{\partial r_i}(\mathbf{r})\right]$$

be the three-dimensional Fourier transformations of the ith component of the gradient of the generating potential. Then after transformation of (9) we obtain, in Cartesian coordinates,

$$\mathcal{F}^3[(\nabla u)^{*2}(\mathbf{r})] = \sum_{i=1}^{3} U_i^2(\mathbf{s}), \tag{10}$$

after application of the correlation theorem.

A4. The transformed partial derivatives

For the three-dimensional Fourier transformation of a partial derivative $\partial u(\mathbf{r})/\partial r_i$ with respect to the ith Cartesian coordinate,

$$U_i(\mathbf{s}) = 2\pi i s_i \, \mathcal{F}^3[u(\mathbf{r})] = 2\pi i s_i \, U(\mathbf{s})$$

is valid. After insertion of this into (10), one obtains

$$\mathcal{F}^3[(\nabla u)^{*2}(\mathbf{r})] = -4\pi^2 s^2 \, U^2(\mathbf{s}). \tag{11}$$

Applying the convolution theorem and (7) to the right side, one obtains the result

$$\mathcal{F}^3[(\nabla u)^{*2}(\mathbf{r})] = -4\pi^2 s^2 \, \mathcal{F}^3[p(\mathbf{r})] = -4\pi^2 s^2 \, I(\mathbf{s}). \tag{12}$$

In scattering physics, the generating potential $u(\mathbf{r})$ is known as the 'density function' from which the scattering is caused. $I(\mathbf{s})$ is the scattered intensity. In the field of SAXS, $u(\mathbf{r}) = \rho_{\rm el}(\mathbf{r}) - \langle\rho_{\rm el}(\mathbf{r})\rangle_v$ is the variation of the electron density about its spatial average.

A5. The Laplacian

The correlation function $p(\mathbf{r})$ itself can be considered a potential, since it is a scalar function of the vector in physical space. For potentials, the Laplacian in Cartesian coordinates is defined by the equation

$$\Delta p(\mathbf{r}) = \sum_{i=1}^{3} \frac{\partial^2 p(\mathbf{r})}{\partial r_i^2}. \tag{13}$$

By applying the definition to (8) and performing the Fourier transformation, one obtains

$$\mathcal{F}^3[\Delta P(\mathbf{r})] = -4\pi^2 s^2 \, I(\mathbf{s}). \tag{14}$$

Comparison with (12) reveals the identity of the right sides. Thus, it follows that the Laplacian applied to the correlation function is equivalent to the autocorrelation of the gradient of the generating potential. In this paper, $\Delta p(\mathbf{r}) = z(\mathbf{r})$ is called the 'generalized chord distribution'.

The Laplacian introduced here is also employed in the fields of digital image processing and in theoretical chemistry for the purpose of analysis of scalar functions. In the field of image processing, it is particularly justified if the image has been blurred by a diffusion process (Rosenfeld & Kak, 1982). In theoretical chemistry, the Laplacian is applied to electron density in order to visualize localized electron pairs (Bader, 1990).

This study has been carried out in the frame of the HASYLAB project II-98-067, 'Polymers with Fibre Symmetry'. The preparation of the sample by E. Buzdugan and P. Ghioca, ICECHIM, Bucharest, in the frame of project RUM-047-97, 'Novel Block-Copolymers with Improved Service Properties', funded by the German and the Romanian Ministries for Education and Research, is gratefully acknowledged. The author gratefully appreciates the helpful discussion of the manuscript with C. Burger and W. Ruland.

References

Bader, R. F. W. (1990). *Atoms in Molecules – A Quantum Theory*. Oxford University Press.
Bonart, R. (1966). *Kolloid Z. Z. Polym.* **211**, 14–33.
Burger, C. & Ruland, W. (2000). Private communication.
Ciccariello, S. (1985). *Acta Cryst.* A**41**, 560–568.
Ciccariello, S. & Benedetti, A. (1986). *J. Appl. Cryst.* **19**, 195–197.
Cohen, Y. & Thomas, E. L. (1987). *J. Polym. Sci. B Polym. Phys.* **25**, 1607–1614.
Elliot, J. A. & Hanna, S. (1999). *J. Appl. Cryst.* **32**, 1069–1083.
Glatter, O. & Kratky, O. (1982). *Small Angle X-ray Scattering*, pp. 26–29. London: Academic Press.
Haberäcker, P. (1989). *Digitale Bildverarbeitung*, pp. 138–139. Munich: Hanser.
Hall, I. H. & Hussain, B. H. (1990). *Colloid Polym. Sci.* **268**, 12–21.
Hall, I. H., Mahmoud, E. A., Carr, P. D. & Geng, Y. D. (1987). *Colloid Polym. Sci.* **265**, 383–393.
IDL (1999). *IDL*. Version 5.3. Research Systems Inc., Boulder, Colorado, USA.
Kumar, S., Warner, S., Grubb, D. T. & Adams, W. W. (1994). *Polymer*, **35**, 5408–5412.
Matlab (2000). *Matlab*. Version 6. The Mathsworks Inc., Natick, Massachusetts, USA.
Méring, J. & Tchoubar, D. (1968). *J. Appl. Cryst.* **1**, 153–165.
Porod, G. (1951). *Kolloid. Z.* **124**, 83–114.
Press, W. H., Teukolsky, S. A., Vetterling, W. T. & Flannery, B. B. (1992). *Numerical Recipes in C*. Cambridge University Press.
pv-wave (1997). *pv-wave*. Version 6.10. Visual Numerics Inc., Boulder, Colorado, USA.
Rosenfeld, A. & Kak, A. C. (1982). *Digital Picture Processing*, Vol. 1, pp. 241–244. London: Academic Press.
Ruland, W. (1971). *J. Appl. Cryst.* **4**, 70–73.
Ruland, W. (1977). *Colloid Polym. Sci.* **255**, 417–427.
Ruland, W. (1978). *Colloid Polym. Sci.* **256**, 932–936.
Ruland, W. (1987). *Macromolecules*, **20**, 87–93.
Siemann, U. & Ruland, W. (1982). *Colloid Polym Sci.* **260**, 999–1010.
Stribeck, N. (1992). *Colloid Polym. Sci.* **270**, 9–16.
Stribeck, N. (1993). *Colloid Polym. Sci.* **271**, 1007–1023.
Stribeck, N. (1999). *J. Polym. Sci. B Polym. Phys.* **37**, 975–981.
Stribeck, N. (2000). *Am. Chem. Soc. Symp. Ser.* **739**, 41–56.
Stribeck, N., Fakirov, S. & Sapoundjieva, D. (1999). *Macromolecules*, **32**, 3368–3378.

Stribeck, N., Ghioca, P. & Buzdugan, E. (1997). *J. Appl. Cryst.* **30**, 708–711.
Stribeck, N. & Ruland, W. (1978). *J. Appl. Cryst.* **11**, 535–539.
Vonk, C. G. (1979). *Colloid Polym. Sci.* **257**, 1021–1032.
Vonk, C. G. & Kortleve, G. (1967). *Kolloid Z. Z. Polym.* **220**, 19–24.
Wolff, T., Burger, C. & Ruland, W. (1994). *Macromolecules*, **27**, 3301–3309.